Robustness of the Half-Metallicity at the Interfaces in Co 2 Mn Si -Based All-Full-Heusler-Alloy Spintronic Devices

B. Pradines, L. Calmels, Rémi Arras

Robustness of the Half-Metallicity at the Interfaces in Co_2MnSi-Based All-Full-Heusler-Alloy Spintronic Devices

B. Pradines, L. Calmels, and R. Arras*

CEMES, CNRS, Université de Toulouse, 29 rue Jeanne Marvig, Toulouse F-31055, France

(Received 3 June 2020; revised 23 December 2020; accepted 4 February 2021; published 3 March 2021)

Based on first-principles methods, we demonstrate that it would be possible to design efficient all-full-Heusler-alloy-based spintronic devices associating Co_2MnSi electrodes and nonmagnetic full-Heusler-alloy spacers selected to preserve the half-metallicity of Co_2MnSi up to the interface atomic layers. We focus on the Co_2MnSi/Fe_2TiSi magnetic tunnel junction, compare the stability range of its different interface terminations, and show that the half-metallicity of the Fe_2/MnSi-terminated interface even withstands atomic intermixing. The robustness of the half-metallicity of this interface termination is also confirmed in Co_2MnSi/Fe_2VAl spin valves. With such interfaces, spintronic devices could possess very high magnetoresistive properties.

DOI: 10.1103/PhysRevApplied.15.034009

I. INTRODUCTION

Known since the beginning of the 20th century, the full-Heusler alloys of general formula X_2YZ have regained a lot of attention when Co_2MnSi, a ferromagnetic crystal with the high Curie temperature of 985 K, has been predicted to be a half-metal [1]. This prediction opened an interesting route towards spintronic devices, such as spin valves (SVs) or magnetic tunnel junctions (MTJs), with exceptional magnetoresistive properties at high temperature. In such devices, the half-metallic Co_2MnSi electrodes are separated by a thin metallic or insulating nonmagnetic spacer and a perfect understanding and mastering of the Co_2MnSi/spacer interfaces is required, to prevent the loss of the half-metallic character at these interfaces. Recent experimental studies have shown that the atomic layer termination of a high crystalline quality Heusler-alloy layer can be measured using the reflection high-energy electron diffraction (RHEED) pattern intensity oscillations, X-ray photoelectron spectroscopy (XPS), and Auger spectra; to a certain extent, the atomic layer termination can also be selected and controlled by choosing the suitable substrate, adjusting the epitaxial growth conditions and precisely counting the number of atomic layers deposited during the layer-by-layer growth process [2,3].

In 1993, Valet and Fert studied the giant magnetoresistance (GMR) of a SV with the current flow perpendicular to the layer planes (CPP configuration) [4]. The CPP-GMR that they calculated depends on two coefficients, which correspond to the bulk magnetic electrode and to the nonmagnetic spacer/ferromagnetic electrode interface contributions to the spin-scattering asymmetry. Both terms are important and the higher they are, the higher the GMR is. Most of the research efforts focused on improving the bulk parameter, searching for electrode materials with a spin polarization at the Fermi level as high as possible (ideally of 100%), and robust with respect to the unavoidable structural defects, like permutations between atoms of different chemical species, which can damage the physical properties in the case of full-Heusler alloys [5–9]. The interface spin-scattering asymmetry coefficient must, however, also be improved to further increase the GMR of SVs based on half-metallic electrodes. More or less empirical rules of thumb have been proposed for that, such as choosing a spacer material, the atomic structure (crystal symmetry, lattice parameter), and band structure (orbital symmetry, dispersion) of which resemble those of Co_2MnSi for majority-spin electrons [10]. The former of these requirements could be reached by using a full-Heusler-alloy spacer instead of the more commonly used Cr [11,12] or Ag [13–15] layer, to prevent the occurrence of interface structural defects and facilitate the epitaxial growth of the multilayers.

Similar arguments apply to the interfaces between Co_2MnSi and the nonmagnetic insulating or semiconducting spacers of Co_2MnSi-based MTJs: the tunnel magnetoresistance (TMR) should increase with the spin polarization at the Fermi level $P(E_F)$ of these interfaces. Interface structural defects (intermixing, deviations from stoichiometry) and possible electron states localized at the interfaces may locally decrease the spin polarization and lower the magnetoresistive properties of these devices. These difficulties in keeping a high spin polarization at the Fermi level near the interfaces between Co_2MnSi and

*remi.arras@cemes.fr

the insulating or semiconducting barrier could be empirically controlled by choosing a suitable spacer material, ideally a full-Heusler alloy (instead of the amorphous AlO_x [16–20], crystalline MgO [21–26], or conventional group IV or III–V semiconductors [27–31]), and by adjusting the growth conditions to select the best interface atomic structure. Note that the interface between Co_2MnSi and a semiconductor can also be used as a spin injector in semiconductor-based spintronic devices [32], another example of application for which a good control of the interface properties is mandatory.

Thanks to the continuity of the atomic structure at their interfaces and owing to the large choice of chemical specie combinations that they offer, Co_2MnSi-based all-full-Heusler-alloy heterostructures should now be investigated to search for the spacer materials leading to SVs and MTJs with the best magnetotransport properties. Few experimental studies have been published on all-full-Heusler-alloy SVs and most of them reported poor GMR values at room temperature [10,33,34]. Such bad performances have mainly been explained in terms of the atomic disorder, such as the Co_{Mn} antisites that may exist in Co_2MnSi electrodes [8]. The possible existence of a dead interface magnetic layer lowering the magnetoresistive performances was moreover reported in the case of Co_2MnGe/Rh_2CuSn SVs [34]. Other Heusler-alloy-based heterostructures have mostly been studied numerically from first principles [35–41]. Chadov *et al.*, in particular, proposed to select the best all-Heusler-alloy MTJs among those which minimize the mismatch between the atomic and the band structures of the electrode and spacer materials: They first decided to select the half-metallic electrode material Co_2MnAl and further proposed to use CoVMnAl as the nonmagnetic insulating spacer [37]. This latter choice results from a modification of the chemical formula of the electrode Heusler alloy, keeping in mind the Slater-Pauling rule. They also suggested that the electronic structure of the $Co_2MnAl/CoVMnAl$ interface resembles that of the interface bulk Heusler alloy (i.e., the compound which can be formed by associating the ultimate atomic layers on both sides of the interface).

In this article, we show that the half-metallic character of Co_2MnSi is preserved at the most stable interfaces with the nonmagnetic semiconductor Fe_2TiSi, in MTJ-like heterostructures. We focus our discussion on the Fe_2/MnSi-terminated interface, for which we show that atomic intermixing is not likely to challenge the half-metallic character of Co_2MnSi, which can then be considered as relatively robust. We finally make a rapid comparison with the Fe_2/MnSi-terminated interface of the SV-like heterostructure that Co_2MnSi can form with the nonmagnetic metallic Heusler alloy Fe_2VAl. The spacer compounds Fe_2TiSi and Fe_2VAl have been selected from their physical characteristics, as described in the database created by Butler *et al.* [42,43].

II. CALCULATION DETAILS

The calculations presented in this paper are based on the density functional theory (DFT) and have been performed with the full-potential linearized augmented plane wave (FPLAPW) code WIEN2K [44]. The exchange and correlation energy was calculated with the generalized gradient approximation (GGA) [45]. Defined as the product of the smallest atomic sphere radius R by the highest reciprocal lattice vector K_{max} of the plane wave expansion, the convergence parameter RK_{max} was set to 7.0, all the atomic sphere radii being fixed to 2.0 atomic units. The irreducible wedge of the first Brillouin zone of the heterostructures was sampled with 156 **k** vectors.

To calculate the electronic and magnetic properties of the $Co_2MnSi/Fe_2TiSi(001)$ and $Co_2MnSi/Fe_2VAl(001)$ heterostructures, we used a supercell that contains 6 bilayers of each material (24 atomic layers in total), stacked along the (001) direction (defined as the z axis) and 2 nonequivalent interfaces. This geometry, depicted in Fig. 1(a), allows a continuity of the Heusler atomic structure across the interfaces and a preservation of the stoichiometry of the two Heusler-alloy layers forming the heterostructures. For each structure, we fixed the in-plane supercell lattice parameter to the equilibrium value calculated for bulk Co_2MnSi, 5.63 Å, whereas the out-of-plane lattice parameter of the supercell and the atom internal coordinates have been optimized by minimizing the ground-state energy and the forces. This choice is motivated by the experimental configuration, where the thin spacer and the top electrode of the corresponding MTJ and SV are epitaxially grown on top of the Co_2MnSi bottom electrode, which imposes its lattice constant.

In Sec. IV B, we discuss the stability of the possible interfaces between Co_2MnSi and Fe_2TiSi, as a function of their interface terminations. Two parameters have been calculated to quantify this stability, i.e., (i) the separation energies E_{sep} and (ii) the interface formation energies γ_{IF}; E_{sep} provides information on the stability of the interface after it has been grown (in fact, on the difficulty to break this interface), γ_{IF} evaluates the ability to experimentally grow the interface.

To compute E_{sep}, we used nonstoichiometric supercells possessing two identical interfaces (either Co_2/TiSi-terminated or Fe_2/MnSi-terminated). Here E_{sep} is defined as the energy difference resulting both from the chemical bonding and the atomic relaxation, when the interface is formed:

$$E_{sep} = E_{Co_2MnSi} + E_{Fe_2TiSi} - E_{HS}, \quad (1)$$

where E_{HS} is the ground-state energy of the heterostructure with symmetric Co_2MnSi and Fe_2TiSi layers and the desired interface termination; E_{Co_2MnSi} and E_{Fe_2TiSi} are the ground-state energies of the isolated nonstoichiometric Co_2MnSi and Fe_2TiSi layers with fully relaxed surfaces,

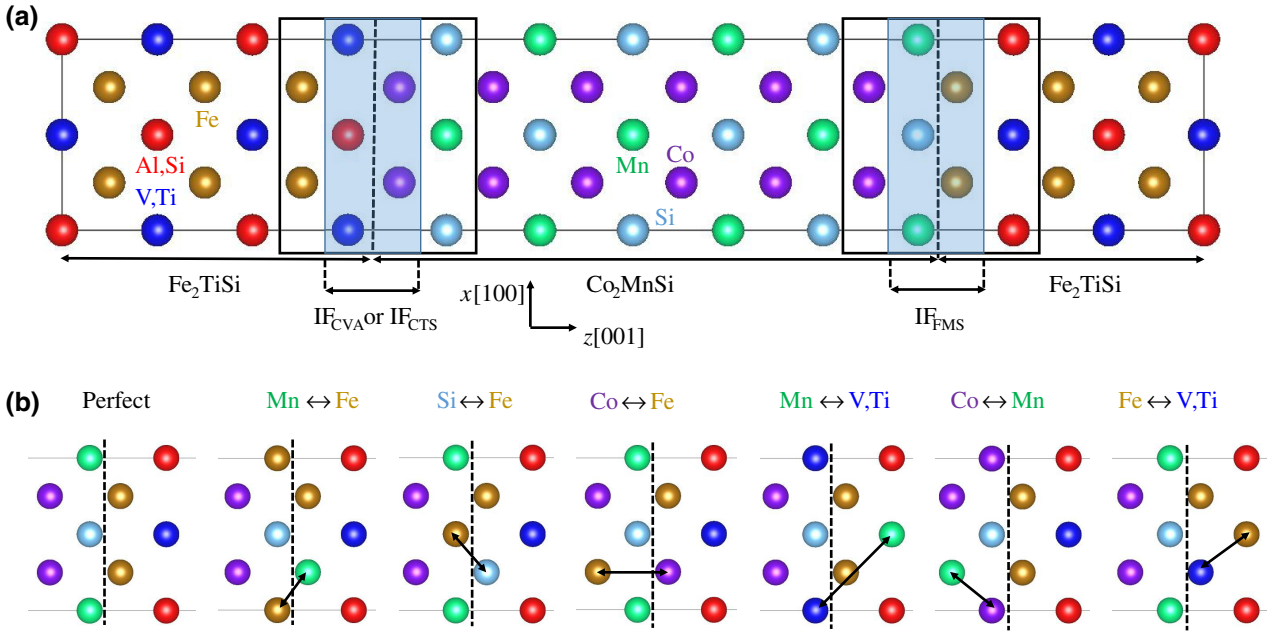

FIG. 1. (a) Atomic structure of the Co_2MnSi/Fe_2TiSi and Co_2MnSi/Fe_2VAl supercells used for the calculations. The light gray boxes show the ultimate atomic layers on both sides of the two nonequivalent interfaces: $Co_2/TiSi$ (IF_{CTS}) or Co_2/VAl (denoted as IF_{CVA}) on the left-hand side, and $Fe_2/MnSi$ (IF_{FMS}) on the right-hand side of the Co_2MnSi thick layer. The solid-line boxes show the atomic bilayers on both sides of these interfaces. (b) Atomic defects which have been considered near the $Fe_2/MnSi$-terminated interfaces.

keeping however the in-plane lattice parameter fixed to the value calculated for Co_2MnSi. This energy is the sum of two contributions: the energy E_{chem} associated to the breaking of the chemical bonds when we separate the two layers and the energy E_{relax} owing to the relaxation of the atomic positions at the two bare surfaces that are created. With this definition, E_{sep} does not provide information on the elastic energy stored in the Fe_2TiSi layer.

The interface formation energies γ_{IF} have been calculated as a function of the chemical potential of the different chemical species constituting the Heusler alloys (these chemical potentials can be changed experimentally by adjusting the growth conditions). A comparison between the different interface energies provides information on the chemical potential ranges for which a particular interface termination is more likely to be formed. The detailed procedure that is used to calculate γ_{IF} is described in the Appendix. For these calculations only, we used the Vienna *ab initio* simulation package (VASP) [46,47] with the projector augmented wave (PAW) method [48].

The values of the spin polarization at the Fermi level $P(E_F)$ can be computed from the equation

$$P(E_F) = \frac{n^{\uparrow}(E_F) - n^{\downarrow}(E_F)}{n^{\uparrow}(E_F) + n^{\downarrow}(E_F)}, \qquad (2)$$

where $n^{\uparrow}(E_F)$ and $n^{\downarrow}(E_F)$ respectively correspond to the majority- and minority-spin densities of states (DOS) at the Fermi level. This description of $P(E_F)$ is, in general, suitable to analyze electronic structure data measured from spin-polarized photoemission experiments. Another definition has been proposed to calculate the degree of spin polarization at the Fermi level, from majority and minority spin current densities instead of DOS [49]. This alternative definition is certainly more relevant to discuss the magnetotransport properties of spintronic devices with conventional ferromagnetic electrodes. However, in the particular case of Co_2MnSi-based devices, the spin polarization of the Co_2MnSi electrodes is of 100% regardless of the definition of the spin-polarization degree, as long as this material keeps its half-metallic character. This is why we have chosen, in the following sections, to discuss the half-metallicity of the Co_2MnSi/nonmagnetic spacer interfaces from the values of $P(E_F)$ computed with $n^{\uparrow}(E_F)$ and $n^{\downarrow}(E_F)$.

An important goal of this paper is to check the robustness of the half-metallicity of the $Fe_2/MnSi$-terminated interfaces of $Co_2MnSi/Fe_2TiSi(001)$ and $Co_2MnSi/Fe_2VAl(001)$ heterostructures. To do so, we built different atomic structures by swapping some of the atoms the closest from the interface, as described in Fig. 1(b); as all the supercells have the same stoichiometry, the creation energy E_c of an intermixing defect is simply given by the ground-state energy difference between the perfect and the defective heterostructures. We mostly considered the atomic exchanges which are the most expected to affect the half-metallicity of the Co_2MnSi interface,

keeping in mind the consequences of such defects in bulk full-Heusler alloys [9]: five of the six disorder scenarios that we consider involve atomic exchanges, either between first- or second-neighbor transition-metal atoms across the interface, or between first-neighbor transition-metal atoms in one or the other side of the interface. The last scenario concerns the possible exchange between first-neighbor Fe and Si atoms across the interface.

III. PHYSICAL PROPERTIES OF THE ELECTRODE, SPACER, AND INTERFACE BULK HEUSLER ALLOYS

A. Physical properties of the electrode (Co_2MnSi) and spacer (Fe_2VAl and Fe_2TiSi) bulk compounds

The calculated physical properties of the electrode (Co_2MnSi) and spacer (Fe_2VAl and Fe_2TiSi) bulk Heusler alloys are summarized in Table I. As expected, Co_2MnSi is ferromagnetic, with a total spin magnetic moment of 5.0 μ_B per formula unit (f.u.), whereas Fe_2VAl and Fe_2TiSi are nonmagnetic, in agreement with the Slater-Pauling equation $m_{\text{spin}} = |24 - N_t|$, where m_{spin} is the spin magnetic moment and $N_t = 29$ for Co_2MnSi and 24 for Fe_2VAl and Fe_2TiSi is the number of valence electrons per f.u. [1,50].

The DOS curves displayed in Fig. 2 confirm that Co_2MnSi is half-metallic, with a minority-spin electron band gap of 0.83 eV, whereas majority spin dispersive bands cross the Fermi level E_F. Fe_2VAl is metallic and Fe_2TiSi is semiconducting with a band gap width of 0.37 eV and both compounds are nonmagnetic. The equilibrium lattice parameters calculated for Fe_2VAl and Fe_2TiSi are 5.69 Å and 5.68 Å, respectively: these materials display a lattice mismatch of only 1% with Co_2MnSi (5.63 Å). All these values are in agreement with the data provided in the previously mentioned database [42].

B. Physical properties of the bulk interface compounds (Co_2TiSi, Fe_2MnSi and Co_2VAl)

For further comparisons, we consider now the two bulk Heusler alloys Co_2TiSi and Fe_2MnSi, which correspond to the chemical formula of the two possible interface terminations of the Co_2MnSi/Fe_2TiSi MTJ; similarly, we also define the interface Heusler alloys Fe_2MnSi and Co_2VAl for the Co_2MnSi/Fe_2VAl SV.

Table I indicates that the lattice parameter of Fe_2MnSi is only 0.9% lower than that of Co_2MnSi, whereas those of Co_2TiSi and Co_2VAl are 2% higher. These differences suggest that structural distortions can be expected to be smaller at the $Fe_2/MnSi$-terminated interface than at the $Co_2/TiSi$- and Co_2/VAl-terminated interfaces.

The DOS of the bulk interface compounds are represented in the bottom panels of Fig. 2: Fe_2MnSi and Co_2TiSi are both half-metallic. Moreover, Fe_2MnSi displays a strong majority-spin DOS peak at the Fermi level, which corresponds to electron states mixing different Co-d and Fe-d orbitals, the largest contribution coming from the Fe-d_{z^2} orbitals. This compound possesses also a total spin magnetic moment of 3.0 μ_B/f.u. and a measured Curie temperature of 219 K [51].

Our calculations predict that Co_2VAl is a nearly half-metallic ferromagnetic metal with a vanishing minority-spin gap, a high $P(E_F)$ of approximately 95.6% and the bottom of the minority-spin conduction band only 0.04 eV below the Fermi level.

The DOS curves that we calculated for the three bulk interface compounds are still in very good agreement with those described in the database of Ref. [42].

If we make the hypothesis that the perfect interfaces should preserve some characteristics of the bulk compounds with the same chemical composition, the DOS curves given in Fig. 2 suggest that the half-metallic character of Co_2MnSi should be preserved at the two possible interfaces of the Co_2MnSi/Fe_2TiSi MTJ, whereas the spin polarization could be lowered at the Co_2/VAl-terminated interface of the Co_2MnSi/Fe_2VAl SV. Following the same hypothesis and by comparing the three possible interface terminations, the $Fe_2/MnSi$ interface appears already as very promising, owing to the mentioned high value of the DOS at the Fermi level for the majority-spin electrons and because of the location of the Fermi level, close to the middle of the band gap for the minority-spin states.

TABLE I. Calculated properties of the relevant bulk full-Heusler alloys: equilibrium lattice parameter a_0, band gap energy at the Fermi level E_g (HM indicates that the material is half-metallic), spin magnetic moment m_{spin} per X_2YZ formula unit (f.u.), and per X, Y, or Z atom.

	a_0 (Å)	E_g (eV)	m_{spin} (μ_B)				Role
			f.u.	X	Y	Z	
Co_2MnSi	5.63	0.83 (HM)	5.00	1.07	2.85	−0.04	Electrode
Fe_2VAl	5.69	0.00	0.00	0.00	0.00	0.00	Spacer
Fe_2TiSi	5.68	0.37	0.00	0.00	0.00	0.00	Spacer
Fe_2MnSi	5.58	0.51 (HM)	3.00	0.25	2.45	−0.02	Interface
Co_2VAl	5.74	0.00	2.00	0.93	0.23	−0.02	Interface
Co_2TiSi	5.74	0.80 (HM)	2.00	1.02	0.00	0.02	Interface

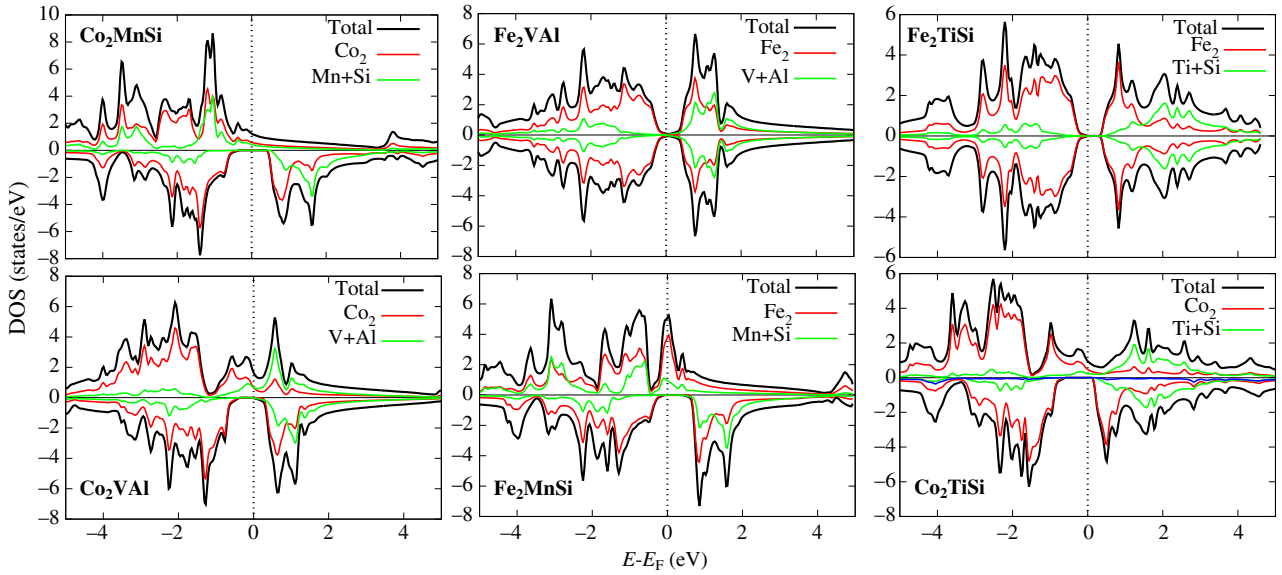

FIG. 2. Top: DOS of the bulk Heusler alloys Co_2MnSi (electrode material), Fe_2VAl and Fe_2TiSi (spacer materials). Bottom: DOS of the bulk interface Heusler alloys: Co_2VAl, Fe_2MnSi and Co_2TiSi. DOS with positive (negative) values correspond to majority (minority) spin projections.

IV. PHYSICAL PROPERTIES OF THE INTERFACES OF THE Co_2MnSi/Fe_2TiSi MAGNETIC TUNNEL JUNCTION

A. Atomic and electronic structures of the perfect interfaces

The relaxation of the atomic positions in the Co_2MnSi/Fe_2TiSi supercell leads to a small [001] tetragonal distortion of the Fe_2TiSi layer: at the center of the Fe_2TiSi layer (i.e., as far as possible from the interfaces), the distance between adjacent atomic layers shows small oscillations around an average value. This latter is slightly (0.5%) larger than the distance between atomic planes in bulk Fe_2TiSi, because of the small compressive stress that the Fe_2TiSi layer undergoes. The distance between nearest-neighbor atomic layers shows larger oscillations when approaching the interfaces, in particular on the Co_2MnSi side of the $Co_2/TiSi$-terminated interface, where it becomes 2–3% higher than in bulk Co_2MnSi. These stronger oscillations have an extension of two or three monolayers on both sides of the interface.

A description of the modifications of the electronic structure of the Heusler alloys induced by the interfaces is provided by Fig. 3. This figure shows the layer-resolved density of states (LDOS) corresponding to the contribution of the two atomic layers on both sides of each of the two nonequivalent interfaces. At the $Co_2/TiSi$-terminated interface [left panels of Fig. 3], the LDOS of the bilayers are very similar to those calculated for bulk Co_2MnSi and bulk Fe_2TiSi and the half-metallicity is preserved at the interface; the main noticeable difference is that the majority-spin LDOS does not exactly vanish on the Fe_2TiSi side of the interface, which also becomes half-metallic. At the $Fe_2/MnSi$-terminated interface [right panels of Fig. 3], the LDOS of the Fe_2 layer is clearly different from that of bulk Fe_2TiSi: a strong LDOS peak is observed above the Femi level for majority spin electrons, which even strengthens the half-metallicity of the heterostructure at this interface. This LDOS peak is a recollection of the majority-spin DOS peak observed at the Fermi level for the bulk interface compound Fe_2MnSi [see Fig. 2].

The calculated spin magnetic moments take almost the same values (within 0.01 μ_B) at the center of the Co_2MnSi layer than in bulk Co_2MnSi. At the $Fe_2/MnSi$-terminated interface, the spin magnetic moment

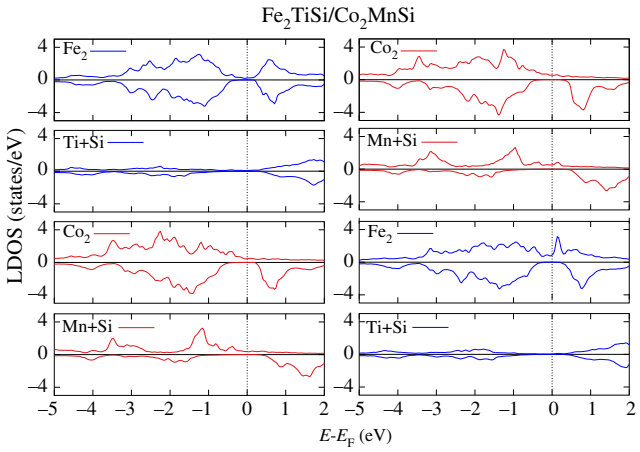

FIG. 3. LDOS for the $TiSi/Co_2$-terminated interface (left panels) and $MnSi/Fe_2$-terminated interface (right panels) of the Co_2MnSi/Fe_2TiSi heterostructure.

of Mn atoms is on average lowered by $-0.22\ \mu_B$, to the advantage of their first-neighbor Fe atoms, of which the spin magnetic moment increases by approximately $0.15\ \mu_B$. At the Co_2/TiSi-terminated interface, the spin magnetic moment of Co atoms and that of their first-neighbor Ti atoms are lowered by $-0.12\ \mu_B$ and $-0.05\ \mu_B$, respectively, whereas the spin magnetic moment of the nearest Fe atoms becomes slightly positive. These modifications of the spin magnetic moments are linked to the charge transfers induced by chemical bonding between atoms on both sides of the interfaces. The sign of these modifications could have been predicted from the variations of the spin magnetic moments between bulk Co_2MnSi and Fe_2TiSi on one side, and the relevant bulk interface compounds Fe_2MnSi and Co_2TiSi, on the other side. The magnetic moment of Fe atoms is for instance $0.25\ \mu_B$ higher in bulk Fe_2MnSi than in bulk Fe_2TiSi (for which it vanishes): this difference is close to the increase of $0.15\ \mu_B$ calculated at the Fe_2/MnSi interface, confirming that the physical properties of the bulk interface Heusler alloys allow to guess those of the atomic layers the closest from the interfaces.

B. Stability domains of the perfect interfaces

At this stage, we must carefully compare the formation energies γ_{IF} of the Co_2/TiSi-terminated and Fe_2/MnSi-terminated interfaces, to predict which is the most likely to be formed with a high crystal quality during the epitaxial growth of a Co_2MnSi/Fe_2TiSi MTJ. As described in the Appendix, the study of the interfaces necessitates first to define the ranges of chemical potentials for which the individual bulk compound are stable and also the stability of their possible surface terminations.

1. Stability of the bulk crystals

Figure 4 displays the stability phase diagrams of bulk Co_2MnSi and Fe_2TiSi. The ranges of chemical potentials for which these Heusler alloys are stable (the white areas in the figure) are determined by comparing their formation enthalpy with those of other possible competing compounds [according to Eq. (A3) in the Appendix], the list of which is established with the help of the Materials Project [52] and Crystallography open databases [53].

2. Relative stability of the Co_2MnSi and Fe_2TiSi surface terminations on top of which the interfaces will be grown

The borders between the stability domains of the Co_2- and MnSi-terminated (001) surfaces of Co_2MnSi and between the stability domains of the Fe_2- and TiSi-terminated (001) surfaces of Fe_2TiSi are represented by blue lines in Figs. 4(a) and 4(b), respectively. These two lines have been calculated from Eq. (A6) in the Appendix. The MnSi and TiSi terminations are more stable (and will be preferentially formed) than the Co_2 and Fe_2 ones

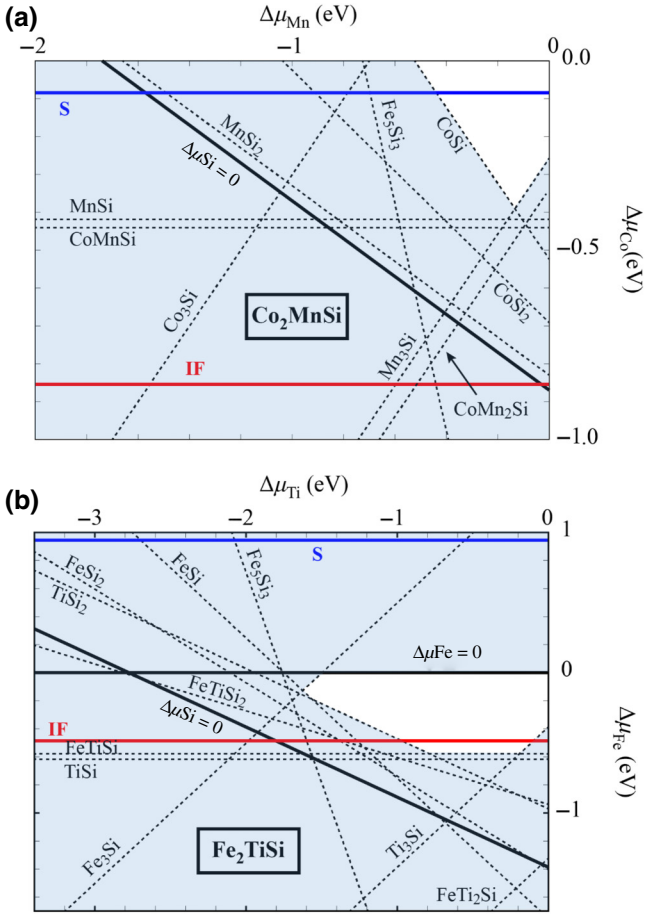

FIG. 4. Stability phase diagrams of (a) Co_2MnSi and (b)Fe_2TiSi. The black dashed lines correspond to the limit for the formation of competitive phases and the white areas correspond to the chemical potential ranges where the Heusler alloys Co_2MnSi and Fe_2TiSi are stable. The blue and red lines delimit the chemical potential ranges of stability of the two possible terminations of the perfect surfaces (S) and of the two possible terminations of the perfect interfaces (IF), respectively.

below these two lines. For Co_2MnSi, we conclude that the Co_2-terminated surface can only be stabilized in Co-rich growth conditions ($\Delta\mu_{Co} > -0.084$ eV), whereas the MnSi-terminated surface will be formed otherwise. This large stability domain of the MnSi-terminated surface has previously been demonstrated in an earlier study [54]. In this latter study, it is interesting to note that it was also suggested that a surface with Mn vacancies could also be formed under Si-rich growth conditions; the study of off-stoichiometric structures is however beyond the scope of our present paper. Figure 4(b) finally shows that only the TiSi-terminated (001) surface of Fe_2TiSi can be grown.

3. Relative stability of the interfaces terminations

We now focus on the determination of the (001) interfaces that can be grown on top of the MnSi-terminated Co_2MnSi surface or on top of the TiSi-terminated Fe_2TiSi

surface. Equation (A7) from the Appendix enables the red line in Fig. 4(a) to be plotted, which delimitates the stability domains of the TiSi/Co_2- and TiSi/MnSi-terminated interfaces grown on Fe_2TiSi. Similarly, the red line in Fig. 4(b) shows the stability domains of the MnSi/Fe_2- and MnSi/TiSi-terminated interfaces. We can conclude from these figures that the MnSi/Fe_2 termination is stable for $\Delta\mu_{Fe} > -0.485$ eV, when Fe_2TiSi is grown on top of the MnSi-terminated Co_2MnSi surface, whereas only the TiSi/Co_2-terminated interface is stable, when Co_2MnSi is grown on top of the TiSi-terminated Fe_2TiSi surface. Co_2MnSi/Fe_2TiSi MTJs can, thus, be grown with the same atomic structure and interface terminations as those used in Sec. IV A to calculate the electronic structure of these devices, if suitable growth conditions are selected.

4. Additional conditions for avoiding the formation of undesired compounds during the growth of the interfaces

If we consider the interface atomic layers as a Fe_2MnSi or Co_2TiSi Heusler alloy formed locally (as described in Sec. III B), we can specify additional constrains which have to be imposed to the chemical potentials so that these interface terminations can be grown instead of any other compound mixing chemical species from both sides of the interfaces (see the Appendix). To guarantee a continuity of the Heusler structure through the entire heterostructure, we can then conclude that the optimal growth conditions would correspond to the intersection between the ranges of chemical potentials defined in this paragraph with those calculated in the previous paragraph.

The range of Fe- and Ti-chemical potentials that must be used to grow a stable Fe_2-terminated Fe_2TiSi spacer on top the MnSi-terminated $Co_2MnSi(001)$ electrode is represented by the white area located above the red line in Fig. 4(b). These arguments do not take into account the possibility that other compounds mixing Fe atoms from Fe_2MnSi and Mn or Si atoms from the Co_2MnSi surface could also form. To check under which conditions this could be avoided, we have calculated the stability diagram of the ordered interface full-Heusler alloy Fe_2MnSi [see Fig. 5(a)]. It follows that the targeted MnSi/Fe_2 interface bilayer can be grown instead of other competitive phases if $\Delta\mu_{Fe} > -0.175$ eV, which means under Fe-rich growth conditions.

Similarly, we have calculated the stability diagram of the interface Heusler alloy Co_2TiSi: the white area in Fig. 5(b) shows that the TiSi/Co_2 interface bilayer should be stable and that competitive phases containing Ti, Si and Co atoms should not be found at the interface when the Co_2MnSi second electrode is grown on top of the TiSi-terminated Fe_2TiSi spacer, if $\Delta\mu_{Co} > -0.232$ eV (Co-rich growth conditions).

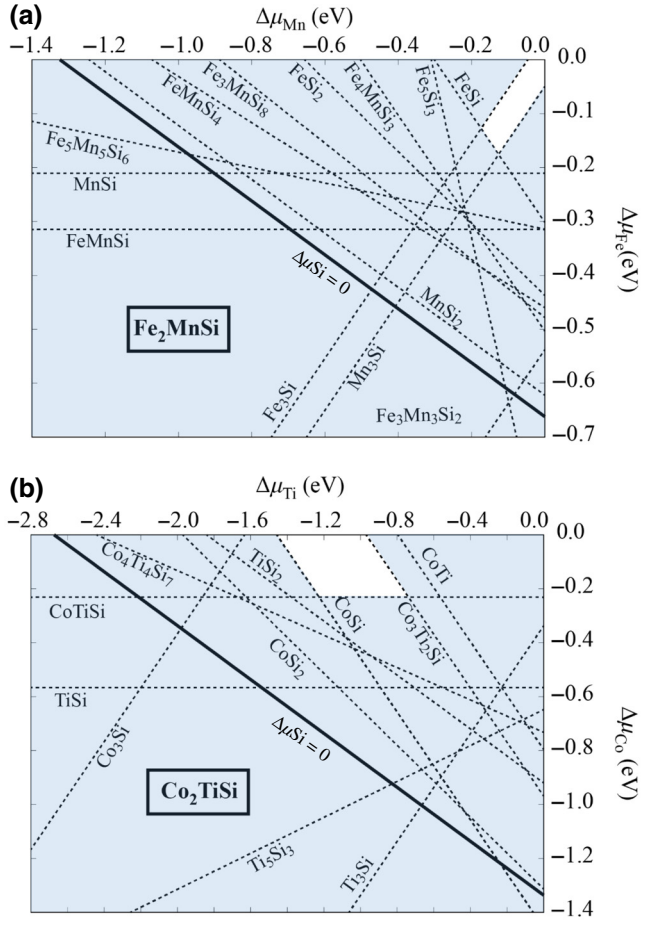

FIG. 5. Stability phase diagrams of the bulk Heusler alloys (a) Fe_2MnSi and (b) Co_2TiSi. The black dashed lines correspond to the limit for the formation of competitive phases and the white areas correspond to the chemical potential ranges where Fe_2MnSi and Co_2TiSi are stable.

5. Robustness of the chemical bonding at the grown interfaces

We can now investigate which of the Fe_2/MnSi- and Co_2/TiSi-terminated interfaces is the most strongly bound. A first response to this question has already been given in Sec. IV A, where we mentioned that the distortions of the atomic structure are larger at the Co_2/TiSi-terminated than at the Fe_2/MnSi-terminated interface, suggesting that the latter could be more stable than the former. Moreover, Table II lists the separation energies for the different interface terminations and we can see that E_{sep} is 0.95 eV (per X_2YZ f.u.) higher for the MnSi/Fe_2-terminated than for the Co_2/TiSi-terminated interface. Such result, however, has to be taken with care, because the definition of E_{sep} considers the separation of the heterostructures into two isolated layers with specific surfaces, which can themselves be more or less stable: interfaces with a termination that involves a Fe_2 atomic layer tend to have a higher E_{sep} energy, because

TABLE II. Separation energies E_{sep} (in eV per X_2YZ f.u.) calculated for different perfect interface terminations of the $Co_2MnSi/Fe_2TiSi(001)$ heterostructure. The meaning of the contributions E_{chem} and E_{relax} are explained in Sec. II.

Termination	E_{chem} (eV)	E_{relax} (eV)	E_{sep} (eV)
$MnSi/Fe_2$	+11.31	−0.69	+10.72
MnSi/TiSi	+6.30	−0.14	+6.16
Co_2/Fe_2	+13.64	−0.93	+12.71
Co_2/TiSi	+10.32	−0.65	+9.77

the Fe_2-terminated surfaces are far less stable than the Co_2-terminated surfaces.

C. Exponential decay in the Fe_2TiSi insulating barrier of the electron states at the Fermi level

The contribution of the successive Fe_2/TiSi bilayers of the barrier to the majority spin DOS at the Fermi level $n^{\uparrow}(E_F)$ decreases exponentially far from the two nonequivalent interfaces, which is due to the fact that a Bloch state with an energy in the band gap of Fe_2TiSi has an imaginary wave number $k = i\kappa$ and cannot propagate in this insulating crystal. As already shown for Fe/MgO/Fe MTJs in the seminal article of Butler *et al.* [55], the distance $d \propto 1/\kappa$ that characterizes this exponential decay only depends on the complex band structure of the insulating spacer and on the symmetry of the metallic electrode Bloch states at the Fermi level: Butler, *et al.*, have for instance shown that Fe Bloch states with the Δ_5 symmetry have a stronger exponential decay than those with Δ_1 symmetry in the MgO barrier of Fe/MgO/Fe MTJs [55].

The z-dependence of the contribution of the successive Fe_2/TiSi bilayers to $n^{\uparrow}(E_F)$ can be described by the general formula:

$$n^{\uparrow}(E_F)(z) = a \times \exp\left(-\frac{z - z_1}{d_1}\right) + b \times \exp\left(\frac{z - z_2}{d_2}\right) \tag{3}$$

where z, z_1, and z_2 are the coordinates of the midpoints between two successive Fe_2 and TiSi atomic layers, between the MnSi and Fe_2 atomic planes of the $MnSi/Fe_2$ interface, and between the TiSi and Co_2 atomic planes of the $TiSi/Co_2$ interface, respectively. Here $d_1 = 0.3a_0$ and $d_2 = 0.7a_0$ are the distances which characterize the exponential decay of $n^{\uparrow}(E_F)$ far from the two interfaces. The fact that $d_1 \neq d_2$ means that the electron states that are responsible for the exponential decays of the Bloch wave functions in the barrier do not have the same symmetry at the two interfaces and that localized interface states are probably involved, at least for one of these interfaces.

A more detailed analysis of the electron states decay, based on the method used by Butler *et al.* for Fe/MgO MTJs [55] or on the calculation of the complex band structure of Fe_2TiSi, is beyond the scope of this paper.

D. Robustness of the half-metallicity of the Fe_2/MnSi-terminated interface with respect to atomic disorder

As it preserves the half-metallic character of Co_2MnSi and presents a DOS peak near the Fermi level, the Fe_2/MnSi-terminated interface should be preferentially selected during the growth process, to get Co_2MnSi/Fe_2TiSi MTJs with improved magnetoresistive properties. Unfortunately, chemical-species disorder and intermixing can hardly be avoided during the growth, in particular when approaching the growth conditions for which other interface terminations could be stabilized.

In the following, we focus on the Fe_2/MnSi-terminated interface and consider the six atomic exchange scenarios displayed in Fig. 1(b), to check whether they may (or not) suppress the half-metallicity, which is predicted up to the ultimate atomic layers for the perfect interface. As mentioned previously, apart from the Fe ⇔ Si exchange across the interface, we only considered atomic disorders between transition-metal atoms located near the interface, as other kinds of disorders (resulting for example from Mn ⇔ Si swaps), already studied for bulk compounds, are not expected to deteriorate the half-metallicity of Co_2MnSi or are not energetically stable [9].

Table III lists the physical properties of the Heusler-alloy atomic bilayers on each side of the six defective Co_2MnSi/Fe_2TiSi interfaces. Fe ⇔ Mn, Co ⇔ Fe and Mn ⇔ Ti intermixing all preserve the half-metallicity of the interface, whereas Fe ⇔ Si exchanges only slightly reduce the spin polarization to 99.8%. Conversely, Ti ⇔ Fe exchanges on the Fe_2TiSi side of the interface and, to a lesser extent, Co ⇔ Mn exchanges on the Co_2MnSi side suppress this half-metallicity. Fortunately, these two defects are not likely to appear, their creation energies being rather high. The half-metallicity of the Fe_2/MnSi-terminated interface can thus be considered as rather robust.

The Co ⇔ Mn exchanges on the Co_2MnSi side of the interface are rather well-known defects in the bulk compound: they correspond to the $D0_3$ disorder, which has already been identified as one of the main causes of the spin depolarization of bulk Co_2MnSi [8,9]. The creation energy of this $D0_3$-like defect located near the interface is nearly the same as that of a $D0_3$ defect in bulk Co_2MnSi (= 1.1 eV/defect when calculated with a $1 \times 1 \times 1$ supercell of 16 atoms); we can thus conclude that the interface does not enhance significantly the probability of obtaining such a defect. In addition to the loss of the half-metallicity, this kind of defect also strongly lowers the spin magnetic moments on the Co_2MnSi side of the interface by 57%. This lowering is local and mainly corresponds to a decrease of the spin magnetic moment of the swapped

TABLE III. Spin polarization $P(E_F)$ and spin magnetic moment M_S calculated per formula unit, for atomic bilayers on the Co_2MnSi and Fe_2TiSi sides of the Co_2MnSi/Fe_2TiSi interface with a $Fe_2/MnSi$ termination. The first and following lines correspond to the perfect and to the defective interfaces, respectively, as proposed in Fig. 1(b). The creation energy E_c of the different defects is given (per defect) in the last column.

Co_2MnSi/Fe_2TiSi					
	$P(E_F)$ (%)		M_S (μ_B/f.u.)		E_c (eV/defect)
	Co_2MnSi	Fe_2TiSi	Co_2MnSi	Fe_2TiSi	
Perfect	100	100	4.73	0.26	...
Fe ⇔ Mn	100	100	4.69	0.37	0.303
Fe ⇔ Si	99.8	99.0	6.40	1.55	2.963
Co ⇔ Fe	100	100	4.54	0.65	0.186
Mn ⇔ Ti	100	100	3.28	1.68	0.203
Co ⇔ Mn	91.7	97.3	2.02	0.36	1.015
Ti ⇔ Fe	36.8	18.9	4.53	1.88	2.258

Mn atom from 2.85 μ_B to −0.78 μ_B, i.e., to a defect antiferromagnetically coupled with the rest of the lattice, which may be very detrimental for the functional properties of Co_2MnSi.

Finally, the Fe ⇔ Si exchange, which involves first-neighbor atoms across the interface, is the less stable of the defects that we considered. It is responsible for a local increase of the magnetic moments on both sides of the interface. The low stability (high creation energy) of this disorder is similar to that of the Co ⇔ Si exchange in bulk Co_2MnSi (see Ref. [9]); this is probably why such disorders have never been reported in experiments. The global increase of the magnetic moment induced by Fe ⇔ Si exchanges is mostly due to a large increase of the Fe magnetic moment, up to 1.11 μ_B on the Fe_2TiSi side of the interface (a value close to the magnetic moment of the Co atoms), and up to 2.64 μ_B on the Co_2MnSi side (a value close to the magnetic moment of the Mn atoms).

V. PHYSICAL PROPERTIES OF THE INTERFACES OF THE Co_2MnSi/Fe_2VAl SPIN VALVE

We have performed a similar analysis on the interfaces of the Co_2MnSi/Fe_2VAl SV and the results we obtained are briefly summarized in the following. The $Fe_2/MnSi$-terminated interface shows smaller structural distortions than the Co_2/VAl-terminated interface, but in contrast to the case of the Co_2MnSi/Fe_2TiSi MTJ, the Co_2MnSi layer loses its half-metallic character in its ultimate atomic bilayer at the $Fe_2/MnSi$-terminated interface. The spin polarization is however still very high in this bilayer, around 98.4%. SVs based on this nearly half-metallic interface thus remain very interesting and should present very high magnetoresistive properties. As the bulk interface Heusler alloy Co_2VAl is nearly half-metallic, the Co_2/VAl-terminated interface also shows a very strong spin polarization at the Fermi level, as we can see in Fig. 6, where the LDOS is represented for the bilayers on both sides of the two interfaces. The LDOS at the atomic layers of the Co_2/VAl-terminated interface are very similar to those calculated respectively for bulk Co_2MnSi and bulk Fe_2VAl. The LDOS of the Fe_2 layer the closest from the $Fe_2/MnSi$-terminated interface is rather different from that of the Fe_2 layer in bulk Fe_2TiSi and presents a rather intense DOS peak just above the Fermi level.

As for the previous heterostructure, we have considered the effects of different kinds of atomic disorders (Fe ⇔ Mn, Fe ⇔ Si, Co ⇔ Fe, Mn ⇔ V, Co ⇔ Mn, or V ⇔ Fe exchanges) at the $Fe_2/MnSi$-terminated interface of the Co_2MnSi/Fe_2VAl SV. As indicated in Table IV, the atomic intermixing responsible for the strongest decrease of $P(E_F)$ in the Co_2MnSi bilayer the closest from the interface are Co ⇔ Mn exchanges on the Co_2MnSi side of the interface and to a lower extent, V ⇔ Fe exchanges on the Fe_2VAl side. However, these two kinds of defects are those with the highest creation energy and are thus less likely to exist at this interface.

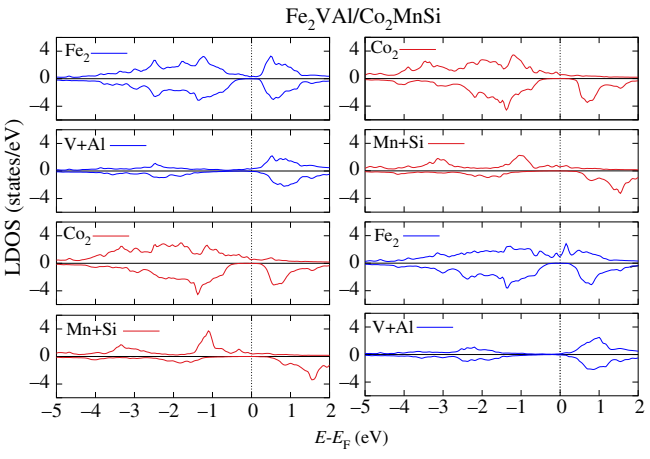

FIG. 6. LDOS for the two atomic layers on both sides of the Co_2/VAl-terminated interface (left panels) and $Fe_2/MnSi$-terminated interface (right panels) of the Co_2MnSi/Fe_2VAl heterostructure.

TABLE IV. Spin polarization $P(E_F)$ and spin magnetic moment M_S calculated per formula unit, for atomic bilayers on the Co_2MnSi and Fe_2VAl sides of the Co_2MnSi/Fe_2VAl interface with a $Fe_2/MnSi$ termination. The first and following lines correspond to the perfect and to the defective interfaces, respectively. The creation energy E_c of the different defects is given (per defect) in the last column.

Co_2MnSi/Fe_2VAl					
	$P(E_F)$ (%)		M_S (μ_B/f.u.)		E_c (eV/defect)
	Co_2MnSi	Fe_2VAl	Co_2MnSi	Fe_2VAl	
Perfect	98.4	89.4	4.68	0.27	...
Fe ⇔ Mn	91.7	88.4	4.64	0.43	0.237
Fe ⇔ Si	95.2	96.4	6.29	1.61	2.456
Co ⇔ Fe	99.1	94.3	4.48	0.67	0.162
Mn ⇔ V	97.1	97.3	3.33	1.62	0.317
Co ⇔ Mn	-0.3	58.1	3.01	0.60	0.981
V ⇔ Fe	86.5	58.0	4.32	0.98	1.361

VI. CONCLUSIONS

In this study, we have performed the numerical investigation of the interface properties of two all-full-Heusler-alloy spintronic devices, the $Co_2MnSi/Fe_2TiSi(001)$ MTJ and the $Co_2MnSi/Fe_2VAl(001)$ SV. These two systems have in common to possess a robust half-metallic electrode and a $Fe_2/MnSi$ termination of their interfaces, which should guarantee the preservation of this half-metallicity up to the insulating layer. We have, moreover, shown that this interface termination can be stabilized when growing the $Co_2MnSi/Fe_2TiSi(001)$ heterojunction, if the proper experimental conditions are chosen.

It is demonstrated that this $Fe_2/MnSi$-terminated interface displays properties similar to those of its stoichiometrically equivalent bulk compound Fe_2MnSi, which can help preserving the half-metallicity of the Co_2MnSi electrode and a significant magnetization up to the interface. A second aspect of this interface is that its half-metallicity remains robust upon the thermodynamically most probable atomic swaps, whereas the atom exchanges that could be detrimental for the interface half-metallicity are less likely to occur. We are thus confident that the $Fe_2/MnSi$-terminated $Co_2MnSi/Fe_2TiSi(001)$ and $Co_2MnSi/Fe_2VAl(001)$ heterostructures could be used in spintronic devices if a good control of the stoichiometry and of the continuity of the full-Heusler crystal structure can be achieved. They should guarantee a strong interface spin polarization at the Fermi level, which is a highly sought property to obtain the highest TMR or GMR values.

The calculated DOS curves also confirm that the other possible interface terminations ($Co_2/TiSi$ or Co_2/VAl) are not expected to destroy the half-metallicity. Such interfaces, or those of other all-full-Heusler-alloy heterostructures, are thus worth being studied. $Co_2/TiSi$-terminated interfaces could for instance present locally a combination of Weyl semi-metallicity and half-metallicity, as predicted for the corresponding bulk compound Co_2TiSi [56].

ACKNOWLEDGMENTS

This work was granted access to the HPC resources of CALMIP (allocation P1252).

APPENDIX: INTERFACE FORMATION ENERGY

In this appendix, we describe the method used to calculate the formation energy of the possible interfaces of the Co_2MnSi/Fe_2TiSi heterostructure. These calculations are made in four steps:

1. First, we calculate the chemical potential range for which each of the two constitutive Heusler alloys X_2YZ is stable.
2. We then consider each of the two compounds independently and calculate which surface termination, $X_2(001)$ or $YZ(001)$, is the most stable.
3. We determine the interface that is preferentially formed when growing the second Heusler alloy on the most stable surface of the first one.
4. We finally propose additional conditions to guarantee that the interface preserves the full-Heusler-alloy structure and the selected stoichiometry.

1. Formation enthalpy of a X_2YZ bulk Heusler alloy

The formation enthalpy ΔH_f^{bulk} of the bulk Heusler alloy X_2YZ can be expressed as

$$\Delta H_f^{\text{bulk}}(X_2YZ) = E_{X_2YZ}^{\text{bulk}} - \sum_{i=X,Y,Z} N_i E_i^{\text{bulk}} \qquad \text{(A1)}$$

where $E_{X_2YZ}^{\text{bulk}}$ is the ground state energy per formula unit calculated for the X_2YZ compound, E_i^{bulk} ($i = X, Y, Z$) are the chemical potentials of the X, Y, or Z atoms in their pure solid phases, $N_X = 2$ and $N_Y = N_Z = 1$.

Considering that the chemical potentials of the atoms of the X_2YZ compound differ from the energies E_i^{bulk} of the pure element bulk crystals by an energy $\Delta\mu_i$, which

depends on the growth conditions, i.e., $\mu_i = E_i^{\text{bulk}} + \Delta\mu_i$, the stability condition of the bulk Heusler alloy X_2YZ is given by

$$2\Delta\mu_X + \Delta\mu_Y + \Delta\mu_Z = \Delta H_f^{\text{bulk}}(X_2YZ) \tag{A2}$$

This equation enables $\Delta\mu_Z$ to be expressed in terms of $\Delta\mu_X$ and $\Delta\mu_Y$.

To grow a X_2YZ compound, it is also necessary to respect the following set of conditions, to avoid that any competitive phase $X_xY_yZ_z$ is formed, instead of X_2YZ:

$$x\Delta\mu_X + y\Delta\mu_Y + z\Delta\mu_Z \leq \Delta H_f^{\text{bulk}}\left(X_xY_yZ_z\right) \tag{A3}$$

When all the possible competitive phases have been considered, we can calculate a phase diagram by identifying the ranges of $(\Delta\mu_Y, \Delta\mu_X)$ where X_2YZ can be formed.

2. Surface energy and surface termination

As in Ref. [54], we consider a symmetric slab of the full-Heusler alloy X_2YZ, with two identical surfaces. The energy γ_S of a surface S is given by

$$\begin{aligned}\gamma_S &= \frac{1}{2A}\left[E_{\text{slab}} - \sum_i N_i\mu_i\right] \\ &= \frac{1}{2A}\left[\Delta H_f^{\text{slab}} - \sum_i N_i\Delta\mu_i\right]\end{aligned} \tag{A4}$$

where E_{slab} is the total energy of the X_2YZ slab with two identical surfaces of area A and ΔH_f^{slab} is the formation enthalpy of the slab, defined as $\Delta H_f^{\text{slab}} = E_{\text{slab}} - \sum_i N_i E_i^{\text{bulk}}$, with $i = X, Y, Z$.

If we consider two films of the same X_2YZ Heusler alloy, with the same thickness but different surface terminations, either X_2 or YZ, we can use the relation

$$\begin{aligned}&\gamma_{(S=X_2)} > \gamma_{(S=YZ)} \\ \Leftrightarrow\ &\Delta H_f^{\text{slab},S=X_2} - 2\Delta\mu_X > \Delta H_f^{\text{slab},S=YZ} - \Delta\mu_Y - \Delta\mu_Z\end{aligned} \tag{A5}$$

to get the chemical potential ranges where the YZ-terminated surface is more stable than the X_2-terminated surface. Using Eq. (A1), this condition can also be written:

$$\begin{aligned}&\gamma_{(S=X_2)} > \gamma_{(S=YZ)} \\ &\quad\text{if} \\ &\Delta\mu_X < \frac{1}{4}\left[\Delta H_f^{\text{slab},S=X_2} - \Delta H_f^{\text{slab},S=YZ} + \Delta H_f^{\text{bulk}}(X_2YZ)\right]\end{aligned} \tag{A6}$$

3. Interface-termination relative stability

It is now possible to calculate the formation energy of the interface resulting from the growth of the Heusler alloys $X_2'Y'Z'$ on the stable surface of the Heusler alloy X_2YZ; because we have already checked the stability of the surface of the Heusler alloy X_2YZ, we only need to consider the growth of $X_2'Y'Z'$. Following the same arguments as in the previous section, the relationship between the interface energies γ_{IF} that corresponds to a X_2'- and to a $Y'Z'$-interface termination on the already grown X_2YZ layer is given by

$$\begin{aligned}&\gamma_{(\text{IF}=X_2')} > \gamma_{(\text{IF}=Y'Z')} \\ &\quad\text{if} \\ &\Delta\mu_{X'} < \frac{1}{4}[\Delta H_f^{\text{slab},IF=X_2'} \\ &\qquad - \Delta H_f^{\text{slab,IF}=Y'Z'} + \Delta H_f^{\text{bulk}}\left(X_2'Y'Z'\right)]\end{aligned} \tag{A7}$$

This equation can be used to determine the chemical potential ranges where the $Y'Z'/YZ$-terminated interface is more stable than the X_2'/YZ-terminated interface. The previously mentioned method is consistent with those proposed in Ref. [57].

4. Preservation of the full-Heusler-alloy structure at the interfaces

As described in the main text, we considered that the association of the YZ and X_2' atomic monolayers of the YZ/X_2'-terminated interface corresponds to the local growth of the $X_2'YZ$ Heusler alloy. Following the same procedure as described in Appendix A 1, we can then define the ranges of chemical potentials where this Heusler alloy can be formed instead of competitive phases. These ranges of chemical potentials add extra constraints to select the appropriate experimental growth conditions.

The ranges of chemical potentials which should be reached when growing the interface thus correspond to the intersection between the domains defined in this section and those calculated from Appendix A 3.

[1] I. Galanakis, P. H. Dederichs, and N. Papanikolaou, Slater-pauling behavior and origin of the half-metallicity of the full-Heusler alloys, Phys. Rev. B **66**, 174429 (2002).

[2] C. J. Palmstrøm, Heusler compounds and spintronics, Prog. Cryst. Growth Charact. Mater. **62**, 371 (2016).

[3] S. Andrieu, A. Neggache, T. Hauet, T. Devolder, A. Hallal, M. Chshiev, A. M. Bataille, P. Le Fèvre, and F. Bertran, Direct evidence for minority spin gap in the Co_2MnSi Heusler compound, Phys. Rev. B **93**, 094417 (2016).

[4] T. Valet and A. Fert, Theory of the perpendicular magnetoresistance in magnetic multilayers, Phys. Rev. B **48**, 7099 (1993).

[5] M. P. Raphael, B. Ravel, Q. Huang, M. A. Willard, S. F. Cheng, B. N. Das, R. M. Stroud, K. M. Bussmann, J. H. Claassen, and V. G. Harris, Presence of antisite disorder and its characterization in the predicted half-metal Co_2MnSi, Phys. Rev. B **66**, 104429 (2002).

[6] B. Ravel, M. P. Raphael, V. G. Harris, and Q. Huang, EXAFS and neutron diffraction study of the Heusler alloy Co_2MnSi, Phys. Rev. B **65**, 184431 (2002).

[7] Y. Miura, K. Nagao, and M. Shirai, Atomic disorder effects on half-metallicity of the full-Heusler alloys $Co_2(Cr_1\text{-}xFe_x)Al$: A first-principles study, Phys. Rev. B **69**, 144413 (2004).

[8] S. Picozzi, A. Continenza, and A. J. Freeman, Role of structural defects on the half-metallic character of Co_2MnGe and Co_2MnSi Heusler alloys, Phys. Rev. B **69**, 094423 (2004).

[9] B. Pradines, R. Arras, I. Abdallah, N. Biziere, and L. Calmels, First-principles calculation of the effects of partial alloy disorder on the static and dynamic magnetic properties of Co_2MnSi, Phys. Rev. B **95**, 094425 (2017).

[10] K. Nikolaev, P. Kolbo, T. Pokhil, X. Peng, Y. Chen, T. Ambrose, and O. Mryasov, "All-Heusler alloy" current-perpendicular-to-plane giant magnetoresistance, Appl. Phys. Lett. **94**, 222501 (2009).

[11] K. Yakushiji, K. Saito, S. Mitani, K. Takanashi, Y. K. Takahashi, and K. Hono, Current-perpendicular-to-plane magnetoresistance in epitaxial $Co_2MnSi/Cr/Co_2MnSi$ trilayers, Appl. Phys. Lett. **88**, 222504 (2006).

[12] Y. Sakuraba, T. Iwase, K. Saito, S. Mitani, and K. Takanashi, Enhancement of spin-asymmetry by $L2_1$-ordering in $Co_2MnSi/Cr/Co_2MnSi$ current-perpendicular-to-plane magnetoresistance devices, Appl. Phys. Lett. **94**, 012511 (2009).

[13] T. Furubayashi, K. Kodama, H. Sukegawa, Y. K. Takahashi, K. Inomata, and K. Hono, Current-perpendicular-to-plane giant magnetoresistance in spin-valve structures using epitaxial $Co_2FeAl_{0.5}Si_{0.5}/Ag/Co_2FeAl_{0.5}Si_{0.5}$ trilayers, Appl. Phys. Lett. **93**, 122507 (2008).

[14] T. Iwase, Y. Sakuraba, S. Bosu, K. Saito, S. Mitani, and K. Takanashi, Large interface spin-asymmetry and magnetoresistance in fully epitaxial $Co_2MnSi/Ag/Co_2MnSi$ current-perpendicular-to-plane magnetoresistive devices, Appl. Phys. Express **2**, 063003 (2009).

[15] J. Sato, M. Oogane, H. Naganuma, and Y. Ando, Large magnetoresistance effect in epitaxial $Co_2Fe_{0.4}Mn_{0.6}Si/Ag/Co_2Fe_{0.4}Mn_{0.6}Si$ devices, Appl. Phys. Express **4**, 113005 (2011).

[16] K. Inomata, S. Okamura, R. Goto, and N. Tezuka, Large tunneling magnetoresistance at room temperature using a Heusler alloy with the *B*2 structure, Jpn. J. Appl. Phys. **42**, L419 (2003).

[17] K. Inomata, N. Tezuka, S. Okamura, H. Kurebayashi, and A. Hirohata, Magnetoresistance in tunnel junctions using $Co_2(Cr : Fe)Al$ full Heusler alloys, J. Appl. Phys. **95**, 7234 (2004).

[18] J. Schmalhorst, S. Kämmerer, M. Sacher, G. Reiss, A. Hütten, and A. Scholl, Interface structure and magnetism of magnetic tunnel junctions with a Co_2MnSi electrode, Phys. Rev. B **70**, 024426 (2004).

[19] K. Inomata, S. Okamura, A. Miyazaki, M. Kikuchi, N. Tezuka, M. Wojcik, and E. Jedryka, Structural and magnetic properties and tunnel magnetoresistance for $Co_2(Cr : Fe)Al$ and Co_2FeSi full-Heusler alloys, J. Phys. D **39**, 816 (2006).

[20] M. Oogane, Y. Sakuraba, J. Nakata, H. Kubota, Y. Ando, A. Sakuma, and T. Miyazaki, Large tunnel magnetoresistance in magnetic tunnel junctions using Co_2MnX ($X = Al : Si$) Heusler alloys, J. Phys. D **39**, 834 (2006).

[21] M. Yamamoto, T. Marukame, T. Ishikawa, K. Matsuda, T. Uemura, and M. Arita, Fabrication of fully epitaxial magnetic tunnel junctions using cobalt-based full-Heusler alloy thin film and their tunnel magnetoresistance characteristics, J. Phys. D **39**, 824 (2006).

[22] S. Tsunegi, Y. Sakuraba, M. Oogane, K. Takanashi, and Y. Ando, Large tunnel magnetoresistance in magnetic tunnel junctions using a Co_2MnSi Heusler alloy electrode and a MgO barrier, Appl. Phys. Lett. **93**, 112506 (2008).

[23] T. Ishikawa, S. Hakamata, K.-i. Matsuda, T. Uemura, and M. Yamamoto, Fabrication of fully epitaxial $Co_2MnSi/MgO/Co_2MnSi$ magnetic tunnel junctions, J. Appl. Phys. **103**, 07A919 (2008).

[24] Y. Miura, H. Uchida, Y. Oba, K. Abe, and M. Shirai, Half-metallic interface and coherent tunneling in $Co_2YZ/MgO/Co_2YZ$ ($YZ = MnSi : CrAl$) magnetic tunnel junctions: A first-principles study, Phys. Rev. B **78**, 064416 (2008).

[25] T. Taira, T. Ishikawa, N. Itabashi, K.-i. Matsuda, T. Uemura, and M. Yamamoto, Influence of annealing on spin-dependent tunneling characteristics of fully epitaxial $Co_2MnGe/MgO/Co_{50}Fe_{50}$ magnetic tunnel junctions, Appl. Phys. Lett. **94**, 072510 (2009).

[26] N. Tezuka, N. Ikeda, F. Mitsuhashi, and S. Sugimoto, Improved tunnel magnetoresistance of magnetic tunnel junctions with Heusler $Co_2FeAl_{0.5}Si_{0.5}$ electrodes fabricated by molecular beam epitaxy, Appl. Phys. Lett. **94**, 162504 (2009).

[27] S. Picozzi, A. Continenza, and A. Freeman, First principles study of electronic and magnetic properties of $Co_2MnGe/GaAs$ interfaces, J. Phys. Chem. Solids **64**, 1697 (2003).

[28] S. Picozzi, A. Continenza, and A. J. Freeman, Spin injection at Heusler/semiconductor interfaces: First-principles determination of potential discontinuity and half-metallicity, J. Appl. Phys. **94**, 4723 (2003).

[29] K. Nagao, M. Shirai, and Y. Miura, Ab initio calculations of spin polarization at $Co_2CrAl/GaAs$ interfaces, J. Phys.: Condens. Matter **16**, S5725 (2004).

[30] I. Galanakis, Towards half-metallic interfaces: Co_2CrAl/InP contacts, J. Phys.: Condens. Matter **16**, 8007 (2004).

[31] X. Y. Dong, C. Adelmann, J. Q. Xie, C. J. Palmstrom, X. Lou, J. Strand, P. A. Crowell, J.-P. Barnes, and A. J. Petford-Long, Spin injection from the Heusler alloy Co_2MnGe into $Al_{0.1}Ga_{0.9}As/GaAs$ heterostructures, Appl. Phys. Lett. **86**, 102107 (2005).

[32] R. Farshchi and M. Ramsteiner, Spin injection from Heusler alloys into semiconductors: A materials perspective, J. Appl. Phys. **113**, 191101 (2013).

[33] T. Kubota, M. Oogane, S. Mizukami, H. Naganuma, Y. Ando, and T. Miyazaki, Magnetoresistance effect in Co_2MnSi/semimetallic-Fe_2VAl/CoFe junctions, J. Phys.: Conf. Ser. **266**, 012096 (2011).

[34] R. Knut, P. Svedlindh, O. Mryasov, K. Gunnarsson, P. Warnicke, D. A. Arena, M. Björck, A. J. C. Dennison, A. Sahoo,

S. Mukherjee, D. D. Sarma, S. Granroth, M. Gorgoi, and O. Karis, Interface characterization of Co_2MnGe/Rh_2CuSn Heusler multilayers, Phys. Rev. B **88**, 134407 (2013).

[35] V. Ko, G. Han, J. Qiu, and Y. P. Feng, The band structure-matched and highly spin-polarized Co_2CrZ/Cu_2CrAl Heusler alloys interface, Appl. Phys. Lett. **95**, 202502 (2009).

[36] V. Ko, G. Han, and Y. Feng, Electronic band structure matching for half- and full-Heusler alloys, J. Magn. Magn. Mater. **322**, 2989 (2010).

[37] S. Chadov, T. Graf, K. Chadova, X. Dai, F. Casper, G. H. Fecher, and C. Felser, Efficient Spin Injector Scheme Based on Heusler Materials, Phys. Rev. Lett. **107**, 047202 (2011).

[38] Z. Q. Bai, Y. H. Lu, L. Shen, V. Ko, G. C. Han, and Y. P. Feng, Transport properties of high-performance all-Heusler $Co_2CrSi/Cu_2CrAl/Co_2CrSi$ giant magnetoresistance device, J. Appl. Phys. **111**, 093911 (2012).

[39] Z. Bai, Y. Cai, L. Shen, G. Han, and Y. Feng, High-performance giant-magnetoresistance junctions based on the all-Heusler architecture with matched energy bands and fermi surfaces, Appl. Phys. Lett. **102**, 152403 (2013).

[40] J. G. Azadani, K. Munira, J. Romero, J. Ma, C. Sivakumar, A. W. Ghosh, and W. H. Butler, Anisotropy in layered half-metallic Heusler alloy superlattices, J. Appl. Phys. **119**, 043904 (2016).

[41] S. Yamada, S. Honda, J. Hirayama, M. Kawano, K. Santo, K. Tanikawa, T. Kanashima, H. Itoh, and K. Hamaya, Magnetic properties and interfacial characteristics of all-epitaxial Heusler-compound stacking structures, Phys. Rev. B **94**, 094435 (2016).

[42] W. H. Butler, A. W. Ghosh, K. Munira, T. Lovorn, J. Romero, C. Lample, L. Wilson, J. Ma, Y. Xie, S. Keshavarz, and D. Mildebrath, Heusler database (2016), http://Heusleralloys.mint.ua.edu/.

[43] J. Ma, V. I. Hegde, K. Munira, Y. Xie, S. Keshavarz, D. T. Mildebrath, C. Wolverton, A. W. Ghosh, and W. H. Butler, Computational investigation of half-Heusler compounds for spintronics applications, Phys. Rev. B **95**, 024411 (2017).

[44] P. Blaha, K. Schwarz, G. Madsen, D. Kvasnicka, J. Luitz, *WIEN2K: An Augmented Plane Wave+ Local Orbitals Program for Calculating Crystal Properties*, edited by K. Schwarz (Vienna University of Technology, Austria, 2001).

[45] J. P. Perdew, K. Burke, and M. Ernzerhof, Generalized Gradient Approximation Made Simple, Phys. Rev. Lett. **77**, 3865 (1996).

[46] G. Kresse and J. Hafner, Ab initio molecular-dynamics simulation of the liquid-metal–amorphous-semiconductor transition in germanium, Phys. Rev. B **49**, 14251 (1994).

[47] G. Kresse and J. Furthmüller, Efficient iterative schemes for ab initio total-energy calculations using a plane-wave basis set, Phys. Rev. B **54**, 11169 (1996).

[48] P. E. Blöchl, Projector augmented-wave method, Phys. Rev. B **50**, 17953 (1994).

[49] I. I. Mazin, How to Define and Calculate the Degree of Spin Polarization in Ferromagnets, Phys. Rev. Lett. **83**, 1427 (1999).

[50] J. Kübler, First principle theory of metallic magnetism, Physica B+C **127**, 257 (1984).

[51] T. Nagano, S. Uwanuyu, and M. Kawakami, Magnetic properties of the Fe_2MnSi- and Fe_2VSi-based Heusler alloys, J. Magn. Magn. Mater. **140-144**, 123 (1995).

[52] A. Jain, S. P. Ong, G. Hautier, W. Chen, W. D. Richards, S. Dacek, S. Cholia, D. Gunter, D. Skinner, G. Ceder, and K. A. Persson, Commentary: The materials project: A materials genome approach to accelerating materials innovation, APL Mater. **1**, 011002 (2013).

[53] S. Gražulis, D. Chateigner, R. T. Downs, A. F. T. Yokochi, M. Quirós, L. Lutterotti, E. Manakova, J. Butkus, P. Moeck, and A. Le Bail, Crystallography open database—An open-access collection of crystal structures, J. Appl. Crystallogr. **42**, 726 (2009).

[54] S. J. Hashemifar, P. Kratzer, and M. Scheffler, Preserving the Half-Metallicity at the Heusler Alloy $Co_2MnSi(001)$ Surface: A Density Functional Theory Study, Phys. Rev. Lett. **94**, 096402 (2005).

[55] W. H. Butler, X.-G. Zhang, T. C. Schulthess, and J. M. MacLaren, Spin-dependent tunneling conductance of Fe|MgO|Fe sandwiches, Phys. Rev. B **63**, 054416 (2001).

[56] G. Chang, S.-Y. Xu, H. Zheng, B. Singh, C.-H. Hsu, G. Bian, N. Alidoust, I. Belopolski, D. S. Sanchez, S. Zhang, H. Lin, and M. Z. Hasan, Room-temperature magnetic topological Weyl fermion and nodal line semimetal states in half-metallic Heusler Co_2TiX (X = Si : Ge, or Sn), Sci. Rep. **6**, 38839 (2016).

[57] B. Hülsen, M. Scheffler, and P. Kratzer, Structural Stability and Magnetic and Electronic Properties of $Co_2MnSi(001)/MgO$ Heterostructures: A Density-Functional Theory Study, Phys. Rev. Lett. **103**, 046802 (2009).